Physicochemical Controls on Adsorbed Water Film Thickness in Unsaturated Geological Media

Tetsu K. Tokunaga

Earth Sciences Division, Lawrence Berkeley National Laboratory

1 Cyclotron Road, ms 70-108B

Berkeley, CA 94720

tktokunaga@lbl.gov

Abstract

Adsorbed water films commonly coat mineral surfaces in unsaturated soils and rocks, reducing flow and transport rates. Therefore, it is important to understand how adsorbed film thickness depends on matric potential, surface chemistry, and solution chemistry. Here, the problem of adsorbed water film thickness is examined through combining capillary scaling with the Derjaguin-Landau-Verwey-Overbeek (DLVO) theory. Novel aspects of this analysis include determining capillary influences on film thicknesses, and incorporating solution chemistry-dependent electrostatic potential at air-water interfaces. Capillary analysis of monodisperse packings of spherical grains provided estimated ranges of matric potentials where adsorbed films are stable, and showed that pendular rings within drained porous media retain most of the "residual" water except under very low matric potentials. Within drained pores, capillary contributions to thinning of adsorbed films on spherical grains are shown to be small, such that DLVO calculations for flat surfaces are suitable approximations. Hamaker constants of common soil minerals were obtained to determine ranges of the dispersion component to matric potential-dependent film thickness. The pressure component associated with electrical double layer forces was estimated using the compression and linear superposition approximations. The pH-dependent electrical double layer pressure component is the dominant contribution to film thicknesses at intermediate values of matric potential, especially in lower ionic strength solutions (< 10 mol m^{-3}) on surfaces with higher magnitude electrostatic potentials (more negative than ≈ -50 mV). Adsorbed water films are predicted to usually range in thickness from ≈ 1 to 20 nm in drained pores and fractures of unsaturated environments.

1. Introduction

Adsorbed water films occur in the subsurface under many commonly occurring and important conditions, from unsaturated soils and fractured rocks at Earth's surface, to deep subsurface reservoirs of oil and gas containing brine as the wetting phase. The water phase in unsaturated porous media has long been recognized to be retained by both capillarity and adsorption [*Buckingham*, 1907], with the matric potential representing the saturation-dependent component of its chemical potential resulting from interactions with the porous solid [*Sposito*, 1981]. The matric potential, ψ_m, encompasses adsorptive and capillary influences on the water phase relative to a reference reservoir of identical composition at atmospheric pressure, and is equivalent to the negative of the disjoining or capillary potentials.

Models that incorporate both adsorptive and capillary mechanisms for describing hydraulic properties have been developed [*Or and Tuller*, 1999; *Philip*, 1978; *Sweeney et al.*, 1993; *Tuller et al.*, 1999]. Thicker, capillary-dominated films are capable of supporting high, gravity-driven seepage velocities [*Nimmo*, 2010; *Tokunaga and Wan*, 1997; 2001]. Here, we reserve the term adsorption to denote interactions between water films on flat and convex segments of grain surfaces, beyond the reach of capillary water within roughness features on grain surfaces and at grain-grain contacts. Being very thin relative to capillarity-controlled water in pendular rings at grain contacts and within topographic minima on rough grain surfaces, adsorbed water films contribute very little to the flow of water [*Dullien et al.*, 1989; *Lebeau and Konrad*, 2010; *Tokunaga*, 2009], diffusion of solutes [*Hu and Wang*, 2003], and transport of colloids [*Saiers and Lenhart*, 2003; *Shang et al.*, 2008; *Wan and Tokunaga*, 1997] in unsaturated media.

Although mineral surfaces exhibit rough microtopography, surface roughness invariably encompasses a large fraction of total surface areas associated with microcrystalline faces that are microscopically flat at the nm scale [*Maurice et al.*, 1995; *Teng*, 2004]. Moreover, basic hydraulic analyses of rough surfaces, from the early conceptual treatment in Buckingham's classic paper [*Buckingham*, 1907] to modern quantitative models [*Or and Tuller*, 2000; *Philip*, 1978] require information on adsorbed film thicknesses. Thus, understanding how adsorbed water film thickness depends on physicochemical properties of porous and fractured media will be useful for more mechanistic predictions of unsaturated flow and transport.

Although adsorbed water films are recognized to limit flow and transport, little is understood about their properties under conditions commonly encountered in the subsurface. In this study, several models are examined in order to compare their predictions on a most basic hydraulic property of water films in unsaturated geological media; the dependence of film thickness on matric potential. We begin with considering bulk surface averaged capillary (pendular ring) film thickness estimates in order to quantify the extent to which capillarity contributes to volumetric water contents of unsaturated media. We then consider the range of dispersion (van der Waals) contributions to adsorbed film thickness predicted for several mineral surfaces, and examine several approximate expressions for electrostatic contributions to adsorbed films. Finally, dispersion and electrostatic contributions are combined to provide estimates of adsorbed water film thickness in unsaturated geological media within the framework of the Derjaguin-Landau-Verwey-Overbeek (DLVO) theory. While the DLVO theory has limitations, it has proven capable of predicting a wide variety of interfacial interactions over length scales ranging from about 1 to 100 nm [*Hiemenz and Rajagopalan*, 1997; *Israelachvili*, 1991]. Therefore the DLVO-based results presented here may be useful for understanding how

hydraulic properties of unsaturated media at low water contents are influenced by matric potential, under given combinations of solution chemistry and mineralogy.

2. Macroscopic normalization of water content to surface area

Calculations of matric potential dependent water content on model porous media are instructive for gaining understanding of ranges of bulk film thickness values and their grain-scale dependence. A simple estimate of water film thickness in partially saturated porous media is obtained by normalizing the volumetric water content to specific surface area. This approach is expected to be most suitable at very low water contents, where adsorption is the dominant retention mechanism. Hence, determination of specific surface areas of soils from water vapor adsorption isotherms has been investigated previously [*Orchiston*, 1953; *Quirk*, 1955]. Hydration of exchangeable cations was identified as a problem for applying the Brunauer-Emmett-Teller method to water vapor adsorption measurements for inferring specific surface areas of soils having appreciable clay fractions [*Quirk*, 1955]. At higher water contents, estimates of average film thickness have been obtained through dividing volumetric water contents by specific surface areas [*Miyamoto et al.*, 2005; *Ponizovsky et al.*, 1999]. Such calculations include capillary water retained in pendular rings and depressions on grain surfaces, therefore overestimate true adsorbed film thicknesses. Monodisperse spherical grains of diameter λ in rhombohedral (close) packing serve as a useful reference for calculating capillary water volumes. In this configuration, each grain is in direct contact with 12 nearest-neighbor grains. The matric potential dependent volumetric water content associated with pendular rings is available from analyses of Fisher [*Fisher*, 1926] and Melrose [*Melrose*, 1966], up to a critical value of saturation ($S_c = 0.243$) where pendular rings become interconnected. Dividing these

volumes by the solid surface area per unit volume provides the pendular ring contribution to bulk film thickness during wetting processes, shown for several different grain sizes in Figure 1. It should be noted that because of hysteresis in the moisture characteristic curves, pendular ring discontinuity requires lower (more negative) matric potentials for drainage processes. Practical upper limits on the wetting curves (shown as open circles) exist because expanding pendular rings become interconnected and pores become saturated at sufficiently high (closer to zero) matric potentials. From capillary scaling, magnitudes of matric potentials associated with pendular ring coalescence and pore saturation scale proportionally with surface tension (σ) and inversely with λ [*Miller and Miller*, 1956]. From capillary models for wetting of rhombohedral packs of monodisperse spherical grains [*Fisher*, 1926; *Melrose*, 1966], the scale-dependent critical matric potential limit at which neighboring pendular rings merge occurs at $\psi_c = -9.1\sigma/\lambda$. In other words, the matric potential must have a magnitude of at least $9.1\sigma/\lambda$ in order for adsorbed films to be important in rhombohedral grain packings. The factor 9.1 is important for later understanding the relative importance of interfacial tension on thicknesses of adsorbed films on spherical surfaces, and will be considered later. Rearranging this scaling relation to the form of $\lambda = -9.1\sigma/\psi_c$ identifies the smallest grain size at which pendular rings are discontinuous during wetting processes. Grain sizes larger than this value are low enough in saturation along the wetting curve such that pendular rings are discontinuous, and are indicated along the upper x-axis of Figure 1 and later figures. This upper x-axis provides a simple indicator of the ψ_m-dependent, limiting grain scale for adsorption-dominated hydraulic behavior. It is instructive to compare these pendular ring-based film thickness with values obtained from modification of Langmuir's adsorbed film equation [*Langmuir*, 1938a; *Tokunaga*, 2009], to be discussed later. The adsorbed film thickness relations based on this approach are also plotted in Figure 1, for the

same grain sizes. The comparisons show that calculated average film thicknesses greater than a few nm using the pendular ring volume/area averaging approach on monodisperse media greatly overestimate values of adsorbed film thickness.

The extent to which grain size influences bulk film thickness in model porous media is discernable from inspection of Figure 1. Miller-Miller scaling [*Miller and Miller*, 1956] dependence of pendular ring water volumes on grain size (λ) is evident from the shifts in capillary "thickness" curves. In contrast, aside from controlling characteristic matric potentials at which pore filling and drainage occur, grain size exerts only a small influence on adsorbed water film thicknesses. This reflects the fact that the magnitude of the λ-dependent capillary pressure of adsorbed water is relatively small compared to the matric potentials associated with these low levels of water saturation [*Tokunaga*, 2009].

3. van der Waals films

Dispersion or van der Waals forces arising from dipole-dipole interactions between all phases present in the water film environment (solid substrate, water film, and air as the nonwetting fluid phase) contribute to the potential-dependence of very thin films. Between planar interfaces, the van der Waals interactions result in a disjoining pressure Π dependent on the reciprocal of the third power of film thickness, f, through

$$\Pi_{vdW}(f) = \frac{-A_{132}}{6\pi f^3} \qquad (1)$$

where A_{132} is the Hamaker constant for the interactions between (1) solid substrate, (3) water film, and (2) air. The value of the nonretarded A_{132} can be estimated from A_{ii} of component materials through the combining relation [*Israelachvili*, 1991]

$$A_{132} = \left(\sqrt{A_{11}} - \sqrt{A_{33}}\right)\left(\sqrt{A_{22}} - \sqrt{A_{33}}\right) \quad (2a)$$

which reduces to

$$A_{132} = A_{11} - \sqrt{A_{11}A_{33}} \quad (2b)$$

because of the negligible magnitude of A_{22} for the air phase. With $A_{33} = 3.7 \times 10^{-20}$ J for water [*Hough and White*, 1980], combining equations yield A_{132} for water films on solid substrates in equilibrium with air. As shown in Table 1, reported values of A_{11} for common soil minerals range for 5×10^{-20} to 2×10^{-19}. Calculated A_{132} values on these mineral surfaces range from -6×10^{-21} to -5×10^{-20}, with more negative values indicative of more stable (thicker) water films.

Equating Π with $-\psi_m$ gives the dispersion (van der Waals) component of the matric potential dependence of film thickness on planar surfaces

$$r(\psi_m) = \left[\frac{A_{132}}{6\pi\rho_w g \psi_m}\right]^{1/3} \quad (3a)$$

[*Iwamatsu and Horii*, 1996; *Or and Tuller*, 1999]. Also included in Table 1 is an effective Hamaker constant for soils proposed by Or and Tuller [*Or and Tuller*, 1999], obtained by fitting surface area normalized soil moisture retention data at low water contents to equation (3). It is reasonable that their effective $A_{132} = -6 \times 10^{-20}$ is larger than values of the minerals because it incorporates additional contributions to water retention including capillarity, electric double layer influences and surface hydration influences.

The predicted matric potential dependence of the dispersion component of film thickness on a variety of common soil minerals (using values of A_{132} from Table 1) is shown in Figure 2. These curves span a fairly narrow range of thicknesses, 30 nm down to ≈ 1 nm, over a broad range of matric potentials (-0.1 kPa to -1 MPa). Note also that relative to silica, the clays and

$Fe(OH)_3$ are predicted to retain thicker adsorbed water films through van der Waals interactions. As before, capillary scale-dependence of pore saturation determines whether or not adsorbed water films are possible at any given matric potential, with approximate threshold grain-sizes indicated along the upper x-axis.

Equation (3a) can be modified to include the additional compressive capillary pressure due to the curvature of air-water interfaces coating ideal spherical grains. For the model spherical grains considered here, the impact of interfacial curvature is included through

$$f(\psi_m) = \left[\frac{h_f^3}{6\pi\left(\psi_m - \frac{4\sigma}{\lambda}\right)} \right]^{\frac{1}{3}} \qquad (3b)$$

where σ is the air-water surface tension. Note that the $4\sigma/\lambda$ term simply accounts for the Young-Laplace capillary pressure associated with the air-water interface coating spherical grains. Predicted film thicknesses on spherical SiO_2 grains of different sizes based on equation (3b) are shown in Figure 3. As before, the ψ_m at which pendular rings merge/separate are indicated by open circles on curves. These results suggest that interfacial curvature can significantly affect film thickness at high (less negative) matric potentials. However, such conclusions only apply to isolated grain surfaces. In packings of grains, adsorbed films at high ψ_m are eliminated through pendular ring coalescence and pore-filling. Figure 3 shows that, at low water saturations associated with film-controlled hydraulic properties, effects of interfacial curvature on the van der Waals contribution to film thickness are minor on smooth spherical surfaces. The fact that surface tension and interfacial curvature impart relatively small influences on adsorbed film thicknesses becomes evident from inspection of equation (3b). Recall that adsorbed films are only important as long as ψ_m remains lower than $-9.1\sigma/\lambda$ for wetting processes. Even more

negative values, below -12σ/λ to -18σ/λ, are required for pendular ring separation during drainage processes because of hysteresis [*Haines*, 1930; *Tokunaga et al.*, 2004]. Because the magnitudes of these ψ_m values associated with adsorbed films are significantly greater than 4σ/λ, interfacial curvature has only a small effect on adsorbed film thicknesses in porous media. It should be noted that edge and corner features on microtopography of mineral surfaces present sites with effectively much finer radii of curvature where local surface tension compressing of films is expected. For simplicity, this study is restricted to smooth surfaces, and most of the following analyses will be limited to flat interfaces because the impacts of spherical curvature (-4σ/λ) are small relative to ψ_m representative of drained pores (< -9σ/λ).

4. Electric double layer water films in unsaturated porous media

In addition to the ever-present van der Waals interactions, charge imbalances at interfaces provide an important mechanism for stabilizing water films through requiring the presence of counterions in the hydrating double layer solution to satisfy overall charge neutrality. In partially water-saturated porous media, the distribution of ions within the aqueous phase is affected by charged interfaces and by the spatial extent of the local aqueous phase. Many of the main features of the electrical double layer can be understood by beginning with the 1-dimensional Poisson-Boltzmann equation [*Israelachvili*, 1991; *Verwey and Overbeek*, 1948] for the variation in electrostatic potential ψ_e in symmetric electrolyte solutions along the direction x, normal to the planar soil-water interface

$$\frac{d^2\psi_e}{dx^2} = \frac{2zN_A e}{\varepsilon_r \varepsilon_0}\left[\exp\left(\frac{ze\psi_e}{k_B T}\right) - \exp\left(\frac{-ze\psi_e}{k_B T}\right)\right] \qquad (4a)$$

or

$$\frac{d^2}{dx^2}\psi_e = \frac{2ez^2n_\infty}{\varepsilon_o\varepsilon_r}\sinh\left(\frac{ez\psi_e}{k_BT}\right) \tag{4b}$$

where e is the electron charge, z is the ion valence, n_∞ is the ion concentration (number density) in the bulk solution, ε_o is the vacuum permittivity, ε_r is the dielectric constant of water, k_B is the Boltzmann constant, and T is the Kelvin temperature. A useful spatial reference scale is the electric double layer decay length or Debye length, κ^{-1}, given by

$$\kappa = \sqrt{\frac{2e^2z^2n_\infty}{\varepsilon_o\varepsilon_r k_BT}} \tag{5}$$

This length scale ranges from ≈ 1 nm up to a few 10s of nm in most pore waters, largely varying with the inverse square-root of ionic strength, $I = n_\infty z^2/N_A$, where N_A is the Avogadro constant. It is also convenient to use the dimensionless electrostatic potential $Y_e = ze\psi_e/k_BT$ because of the importance of ψ_e relative to $k_BT/e \approx 26$ mV (T = 298 K). For the conditions to be described, the electrostatic potential at a given surface, $\psi_{e,i}$, will often be expressed in dimensionless form, $Y_{e,i}$. The one-dimensional Poisson-Boltzmann can then be expressed in terms of the dimensionless potential and Debye length as

$$\frac{d^2}{dx^2}Y_e = \kappa^2\sinh Y \tag{4c}$$

A conceptual model of distributions of water and electrostatic potentials in unsaturated porous media is shown in Figure 4.

Within locally capillary-saturated regions with water film thicknesses much greater than κ^{-1}, the aqueous phase electrochemical conditions reflect those of bulk solutions (Figure 4a). These thick, capillarity-dominated regions serve as local reservoirs maintaining constant background aqueous solution chemical conditions (n_∞) where cation and anion charge balance is

retained. Within saturated regions with opposing solid surfaces in much closer proximity (i.e., closest to grain-grain contacts), electric double layers overlap, cation accumulation and anion exclusion become dominant (Figure 4b). When adsorbed films have thicknesses similar to κ^{-1}, these same conditions are expected to be important.

5. Langmuir's model for adsorbed water films

Langmuir developed a simple electric double layer model to describe adsorbed film thicknesses for dilute aqueous solutions in equilibrium on a solid of high (magnitude) surface electrical potential [*Langmuir*, 1938a]. Experimental results discussed later indicate that the dilute solution requirement is met for ionic strengths $\leq 10^{-1}$ mol m^{-3}. Although the required magnitude of ψ_1 was unspecified, inspection of the Poisson-Boltzmann equation shows that $Y_{1,1} > 3$ is satisfactory for applying the Langmuir model. Langmuir equated equilibrium adsorbed water films on single surfaces with water retained within one half-space of a confined volume bounded by opposing identical surfaces, as depicted in comparing Figures 4b and 4c. The dielectric constant of water and valence of ions are the only chemical properties of the aqueous phase used in the Langmuir model, with film thickness predicted to be inversely related to valence on the dominant ionic species. We modified the Langmuir model to describe water films on spherical grain surfaces in order to estimate the hydraulic properties of porous media at low water saturations [*Tokunaga*, 2009; *Wan and Tokunaga*, 1997]. With the inclusion of a capillary scaling term that accounts for surface tension σ and grain diameter λ, acting on the convex film enveloping the grain, the Langmuir equation becomes

$$f(\psi_{1,1}) \quad \left(\frac{\pi k_B T}{2}\right)\left(\frac{\quad}{\quad} - \psi_{1,1}\right)^{2} \tag{6}$$

It should be noted that σ/λ is correctly multiplied by a factor of 4 here, and incorrectly by 2 in the recent paper [*Tokunaga*, 2009]. Thicknesses of dilute aqueous films of monovalent ions based on equation (6) were shown in Figure 1 for a range of grain sizes, again with upper limits associated with pendular ring merging indicated by circles. At low ionic strength, electrostatic influences on 1 mm diameter grain surfaces are predicted to stabilize films at thicknesses below 50 nm. In unsaturated media of smaller grain size, the upper limit on adsorbed film thickness is constrained to even thinner values because of required magnitudes of matric potentials for pore drainage and because of greater convex curvature of grain-coating films. From equation (6), aqueous films of divalent ions are predicted to be half as thick as those for the monovalent cases shown in Figure 1. From inspection of Figures 3 and 1, it is apparent that Langmuir films are thicker than van der Waals films over most of the matric potential range encountered in the subsurface.

Some tests of predictions based on the Langmuir film model are available. Data from Read and Kitchener [*Read and Kitchener*, 1969] for aqueous films with KCl concentrations ranging from 10^{-2} to 1 mol m^{-3}, adsorbed on silica at an equivalent matric potential of -145 Pa, supporting Langmuir's approximation at the lower salt concentrations. Their data also indicate a trend of thinning films with higher ionic strength (Figure 5). Several other experimental investigations yielding thicker films than predicted by the Langmuir equation for $f < 30$ nm [*Israelachvili*, 1991]. A very broad range of confined film pressures has been investigated through experiments on swelling of clays [*Viani et al.*, 1983]. Although such studies are concerned with water films confined between opposing clay interfaces, one can examine these results to test the reliability of Langmuir's original proposition that adsorbed water films are chemically equivalent to water within one half-space of interlayer region between hydrated

clays. The empirical relation developed by Low [*Low*, 1987] to relate Viani et al.'s clay interlayer distances to swelling (disjoining) pressures ranging from 5×10^4 Pa up to 7×10^5 Pa takes the form

$$f(\psi_m) = \frac{k'_\alpha}{\ln\left[\left(-\psi_m + 1.10 \times 10^{-7}\right) B\right]} \tag{7}$$

with k'_α = 4.57 nm and B = 7.9×10^4 Pa for $\psi_m > -2.03 \times 10^5$ Pa, and k'_α = 2.35 nm and B = 1.48×10^5 Pa for $\psi_m < -2.03 \times 10^5$ Pa. Comparison of the Langmuir adsorbed film model to Low's empirical correlation reveals remarkably good agreement over a wide range of matric potentials, i.e., ψ_m more positive than -2×10^5 Pa (Figure 5). The agreement between these relations lends support to use of the Langmuir adsorbed film model for monovalent solutions up to 0.1 mol m^{-3} (experiments on which Low's correlation was developed utilized smectite clays in 0.1 mol m^{-3} NaCl). This agreement also indicates that simple double layer electrostatic considerations (without including van der Waals force) are sufficient to describe the clay swelling behavior at low ionic strength down to half-space distances of a few nm [*Langmuir*, 1938b]. We also include film thickness calculations based on van der Waals forces with an effective Hamaker constant of -6×10^{-20} J [*Or and Tuller*, 1999]. Note that the curves will cross-over at very low matric potentials, where van der Waals forces become dominant [*Lebeau and Konrad*, 2010]. While the Langmuir model is suitable for low ionic strength solutions adsorbed on surfaces of high electrostatic potential, these conditions are fairly restrictive in soils and unsaturated geological formations. Because pore water ionic strength often exceeds 0.1 mol m^{-3} and surface electrostatic potentials are mineral- and solution chemistry-dependent, more general electric double layer models for adsorbed film thicknesses are desirable.

6. Adsorbed water under wider ranges of ionic strength and surface charge density.

The behavior of adsorbed water films under broader ranges of conditions can be explored through direct numerical solutions of the Poisson-Boltzmann equation [*Devereux and de Bryun*, 1963], and a variety of analytical simplifications [*Russel et al.*, 1989]. Analytical approximations offer the advantage of computational simplification, but need to be carefully selected for applicability to problems of interest. The electrostatic potential adjacent to interfaces is constrained between two limiting cases, constant surface potentials [*Ohshima et al.*, 1982] and constant surface charge [*Gregory*, 1975]. The more general intermediate behavior of charge regulation involves variations in both potential and charge density in response to surface reactions resulting from variations in distances between opposing interfaces [*Chan et al.*, 2006; *Lyklema and Duval*, 2005]. Therefore, approximate solutions to the Poisson-Boltzmann equation that predict behavior intermediate to the two limits of constant surface potential and constant surface charge can provide relatively reliable results. Gregory's double layer compression approximation predicts behavior intermediate to the two extremes for oppositely charge opposing surfaces, and behavior much closer to the constant surface charge limit for similarly charged opposing interfaces [*Gregory*, 1975]. It is able to represent interactions with surfaces having low to intermediate magnitude electrostatic potentials over a wide range of surface separations in a moderately wide range of ionic strength solutions. Gregory's compression approximation for the electrostatic contribution to the disjoining pressure, Π_{el}, in a symmetric electrolyte solution confined between charged plates is related to f through

(8)

where $Y_{e,1}$ and $Y_{e,2}$ are dimensionless electrical potentials at opposing interfaces 1 and 2. It should be noted that this approximation is most satisfactory when $Y_{e,i} \leq 2$, or equivalently $\psi_{e,i} < 50$ mV in 1:1 electrolytes (for T = 298 K). If $Y_{e,1} = Y_{e,2}$, configurations similar to those of Langmuir's can be examined for lower magnitudes of surface potential (using $2f$ as the gap distance). By representing the dimensionless electrostatic potential at the solid-water as $Y_{e,1}$ and its value at the water-air interface as $Y_{e,2}$, Gregory's compression model can be used to estimate adsorbed water films up to moderate ionic strength, on surfaces of low to moderate electrostatic potential. Moreover, because opposing interfaces with different surface potentials are accommodated, implications of charging at the air-water interface can be examined.

Another useful approximate relation between matric potential and film thickness follows from the linear superposition approximation (LSA) for pairs of planar double layers. When film thicknesses are large relative to the characteristic double layer thickness ($\kappa f > 1$), interactions between opposing double layers are sufficiently small such that their electrostatic potentials are approximately additive [*Verwey and Overbeek*, 1948]. The pressure in a symmetric electrolyte solution confined between charged plates in the LSA model gives

$$\Pi_{LSA}(f) = 64 n_\infty k_B T \tanh\left|Y_{e,1}/4\right| \tanh\left|Y_{e,2}/4\right| \exp(-\kappa f) \qquad (9)$$

The LSA-predicted pressures are also intermediate to the constant surface potential and constant surface charge based predictions, but closer to the latter [*Gregory*, 1975]. Note that the interfacial tension contribution to film pressure can be included by simply adding $4\sigma/\lambda$ to the left sides of equations (8) and (9). However, as noted earlier, this influence is relatively small.

An important influence on adsorbed water film thicknesses appears to be the electrostatic potential associated with the air-water interface, ψ_{e2} in equations (8) and (9). The possibility that a finite surface potential at the film's air-water interface could influence thickness relations was

raised by Read and Kitchener [*Read and Kitchener*, 1969], although very few measurements of air-water interfacial charge were available at that time. Demonstrations of clay colloid partitioning at air-water interfaces suggest that these interfaces are weakly negatively charged [*Wan and Tokunaga*, 2002]. Since then, a number of investigations into charge and electrical potential at air-water interfaces have been conducted based on air bubble electrophoretic mobility. The data and literature values reported recently [*Najafi et al.*, 2007; *Takahashi*, 2005] exhibit considerable variability, but nevertheless show trends with respect to pH, ion type, and ion concentration. For the 10 mol m^{-3} NaCl solutions, zeta potentials (ζ) decreased from $\approx 0 \pm 10$ mV at pH 2 to 3, to $\approx$ -40 ±20 for pH $\geq$ 8. Within the range of 4 < pH < 8, $\zeta \approx$ -25 ±10 mV. Being associated with the slip plane, values of ζ potentials are lower in magnitude than the electrostatic potential at the air-water interface, $\psi_{e,2}$. Lacking direct measurements of the latter, ζ = 0, -1, -25, and -50 mV will be used as estimates for $\psi_{e,2}$ in some of the following examples.

Specific cases for increased ionic strength (with $\psi_{e,1}$ = -50 mV for the solid-water interface) predicted by the compression model and the LSA are shown in Figure 6, along with Langmuir's model (flat surface limit). For these comparisons, Π_{el} is equated with $-\psi_m$. Film thicknesses less than 1 nm are not plotted because they are below the resolution of these mean field (continuum) approaches. It should be noted that $\psi_{e,2}$ for the air-water interface is set to -1 mV for the LSA for these comparisons because the model requires opposing interfaces with finite potentials of identical sign. These comparisons show that as the requirement of dilute ionic strength solutions employed in Langmuir's model is relaxed, thinner adsorbed water films result. The compression approximation model exhibits thicker films than the LSA because of its greater confinement of counterions between charged surfaces. It should be noted that the predictions from the compression approximation at 0.1 mol m^{-3} approach the Langmuir curve more closely

as $\psi_{e,1}$ is increased to higher magnitudes (not shown). Although an upper limit of $|\psi_{e,1}| \approx 50$ mV ($Y_{e,1} \approx 2$) was recommended for the compression model and LSA [*Gregory*, 1975], Overbeek noted that models based on linear approximations can yield reasonable results up to $|\psi_{e,1}| \approx 100$ mV ($Y_{e,1} \approx 4$) [*Overbeek*, 1990].

The influences of $\psi_{e,1}$ at the solid-water interface on film thickness predicted by the compression and LSA models are shown in Figure 7 for a background ionic strength of 10 mol m^{-3}. For reasons mentioned previously, the electrostatic potential at the air-water interface $\psi_{e,2}$ was limited to -1 mV for the LSA calculations. Again, thicker films are predicted with the compression model relative to the LSA, and both models yield thinner films than the Langmuir model. These results show the importance of surface potential, with higher magnitude $\psi_{e,1}$ stabilizing thicker films because of the requisite higher concentration of counterions required within the film for charge balance. The surface charge density, σ^*, associated with $\psi_{e,1}$ can be calculated from the Grahame equation [*Grahame*, 1953], which for 1:1 electrolyte solutions is

$$\sigma^* = -\sqrt{8\varepsilon_r \varepsilon_0 n_\infty kT} \sinh(Y_{e,1}/2) \tag{10}$$

Based on this relation, the $\psi_{e,1}$ of -10, -50, and -100 mV cases depicted in Figure 7 correspond to surface charge densities of 2, 13, and 40 mC m^{-2} (at an ionic strength of 10 mol m^{-3}). Quartz and colloidal silica exhibit this range of surface properties in solutions ranging from pH 4 to pH 8 [*Dove and Craven*, 2005; *Kitamura et al.*, 1999]. Calculations summarized in Figure 7 also illustrate how the electrostatic component of film thickness diminishes as the pH associated with the point of zero charge (p.z.c.) [*Sposito*, 1998] is approached. At the p.z.c., no variations in counterion concentrations relative to n_∞ are required, hence the mineral surface electric double layer film is fully collapsed.

The final double layer variable to examine is the electrostatic potential at the air-water interface. Based on ζ values noted previously, ψ_e = -25 mV is taken as a reference value for the air-water interface, for interaction with a solid-water interface with ψ_e = -50 mV, in 10 mol m^{-3} bulk solution ionic strength. The film thickness relations obtained from the compression and LSA models are shown in Figure 8 for air-water interface ψ_e values of 0 (or -1), -25, and -50 mV. With a more highly negatively charged air-water interface ψ_e, thicker adsorbed films are supported through repulsive interactions with the negatively charged solid surface. Repulsion will diminish with decreases in negative charge density (or even charge reversal) on both surfaces as pH is decreased. Thus, these models predict generally thinner adsorbed water films at lower pH.

7. Combining van der Waals and electrostatic influences on adsorbed water films

The combination of dispersion and electrostatic forces for predicting interactions between colloidal interfaces is central to DLVO theory, where their associated pressures are commonly treated as additive in colloidal suspensions and mineral-water-oil systems [*Gee et al.*, 1990; *Israelachvili*, 1991; *Low*, 1987; *Russel et al.*, 1989]. Various DLVO analyses have also been developed for adsorbed water films [*Churaev*, 2003; *Novy et al.*, 1989]. However, to our knowledge, application of the DLVO theory to predictions of adsorbed water film thicknesses in porous media while delineating grain scale-dependent ψ_m constraints has not previously been reported. With respect to the matric potential, this additivity takes the form

$$\psi_{m}(h) = -\Pi_{vdW}(h) - \Pi_{el}(h) \tag{11}$$

Here, we combine the dispersion component with two different electrostatic approximations (compression and LSA) in order to estimate the relative contributions of each interaction on flat

solid surfaces. The reference conditions to be illustrated are for water films on an SiO_2 surface with $\psi_{e,1}$ = -50 mV, the air-water interface $\psi_{e,2}$ = -25 mV, and A_{132} = -1.3 x10^{-20} J. Calculations were done for $\psi_m(f)$ using equations (1), (11) and either (8) (compression) or (9) (LSA), then plotted as $f(\psi_m)$ in Figure 9. The ionic strength influence is shown in these figures for 1:1 electrolyte solution concentrations of 1 mol m^{-3} and 100 mol m^{-3}. Comparisons between electrostatic only (compression and LSA) and DLVO (electrostatic plus dispersion) model calculations show that the dispersion contribution is relatively small over most of the plotted matric potential range under the selected surface potentials. However, these graphs do indicate that dispersion is important at low matric potentials in dilute solutions. As expected, the DLVO calculated film thicknesses in the more dilute solution concentration (1 mol m^{-3}) examples approach the Langmuir model predictions. It is also important to recall that, being based on mean field relations, the DLVO calculations have a lower film thickness limit of about 1 nm [*Israelachvili*, 1991; *Ninham*, 1999; *Russel et al.*, 1989; *Verwey and Overbeek*, 1948], which corresponds to a matric potential limit typically in the range of about -10^5 Pa. Also shown on these figures are estimated water film thicknesses at matric potentials of -10^5 and -10^6 Pa in soils studied by Campbell and Shiozawa [*Campbell and Shiozawa*, 1992] and Tuller and Or [*Tuller and Or*, 2005]. These estimates were obtained by dividing gravimetric water contents reported by Campbell and Shiozawa by the product of water density times specific surface area reported by Tuller and Or. Film thicknesses at higher (closer to zero) ψ_m were not calculated from these soil data because of expected greater contributions from capillary water. For reasons described in Tuller and Or [*Tuller and Or*, 2005], the Salkum soil was excluded from this calculation. The remaining five soils yielded estimated film thicknesses of 1.4 to 2.0 nm at ψ_m = -10^5 Pa, and 1.0 to 1.2 nm at ψ_m = -10^6 Pa, in fairly good agreement with the DLVO calculations.

8. Summary

The dependence of water film thickness on matric potential, solution chemistry, and interfacial properties was studied through calculating capillary drainage in model systems, and predicted interfacial interactions under the resulting unsaturated conditions. Dispersion (van der Waals) and electrostatic interactions were determined for conditions representative of many unsaturated soil and rock environments through calculating nonretarded Hamaker constants for adsorbed water films between air and common mineral surfaces, and through applying approximate expressions for electrical double layer pressures, respectively. Together, these contributions yield DLVO relations between film thickness and matric potential. Thinner water films are predicted with higher ionic strength solutions and lower interfacial electrostatic potentials. Therefore, thinner films are also expected when the pore waters have pH close to the PZC of the solid surface. For similar reasons, neutralization of the negative electrostatic potential at the air-water interface at low pH is also expected to cause film thinning. In very dilute solutions on interfaces with higher surface potentials, thicker films are stable and approach the matric potential dependence predicted by the Langmuir model. Under commonly encountered unsaturated zone conditions with moderate ionic strength (≈ 10 mol m^{-3}), moderate mineral surface potentials (≈ -50 mV), and weakly negative electrostatic potential at the air-water interface (≈ -25 mV), the models predict that adsorbed water films will typically have thicknesses ranging from a few nm to about 20 nm. Such thin films limit flow and transport rates in unsaturated geological media.

Acknowledgments. I thank Marc Lebeau and two anonymous reviewers for their thorough, expert reviews and very helpful comments. This work was carried out under U.S. Dept. of

Energy (DOE) Contract No. DE-AC02-05CH11231. Funding provided by the DOE, Basic Energy Sciences, Geosciences Research Program is gratefully acknowledged.

References

Bergstrom, L. (1997), Hamaker constants of inorganic materials, *Adv. Colloid Interface Sci.*, *70*, 125-169.

Berka, M., and J. A. Rice (2004), Absolute aggregation rate constants in aggregation of kaolinite measured by simultaneous static and dynamic light scattering, *Langmuir*, *20*(15), 6152-6157.

Blakey, B. C., and D. F. James (2003), The viscous behaviour and structure of aqueous suspensions of goethite, *Colloids Surf., A*, *231*, 19-30.

Buckingham, E. (1907), Studies on the movement of soil moisture, Bureau of Soils, U. S. Department Agriculture, Government Printing Office, Washington, DC.

Campbell, G. S., and S. Shiozawa (1992), Prediction of hydraulic properties of soils using particle-size distribution and bulk density data, in *Indirect Methods for Estimating the Hydraulic Properties of Unsaturated Soils*, edited by M. T. van Genuchten and F. J. Leij, pp. 317-328, University of California, Riverside, CA.

Chan, D. Y. C., T. W. Healy, T. Supasiti, and S. Usui (2006), Electrical double layer interactions between dissimilar oxide surfaces with charge regulation and Stern-Grahame layers, *J. Colloid Interface Sci.*, *296*, 150-158.

Churaev, N. V. (2003), Surface forces in wetting films, *Adv. Colloid Interface Sci.*, *103*, 197-218.

Derjaguin, B. V., Y. I. Rabinovich, and N. V. Churaev (1978), Direct measurements of molecular forces, *Nature*, *272*, 313-318.

Devereux, O. F., and P. L. de Bryun (1963), *Interactions of Plane-Parallel Double Layers*, Cambridge, MA.

Dove, P. M., and C. M. Craven (2005), Surface charge density on silica in alkali and alkaline earth chloride electrolyte solutions, *Geochim. Cosmochim. Acta*, *69*(21), 4963-4970.

Dullien, F. A. L., C. Zarcone, I. F. Macdonald, A. Collins, and R. D. E. Bochard (1989), The Effects of Surface-Roughness on the Capillary-Pressure Curves and the Heights of Capillary Rise in Glass Bead Packs, *J. Colloid Interface Sci.*, *127*(2), 362-372.

Fisher, R. A. (1926), On the capillary forces in an ideal soil; Correction of the formulae given by W. B. Haines, *Journal of Agrcultural Science*, *16*, 492-505.

French, R. H. (2000), Origins and applications of London dispersion and Hamaker constants in ceramics, *J. Am. Ceram. Soc.*, *83*(9), 2117-2146.

Gee, M. L., T. W. Healy, and L. R. White (1990), Hydrophobic effects in the condensation of water films on quartz, *J. Colloid Interface Sci.*, *140*(2), 450-465.

Grahame, D. C. (1953), Diffuse double layer theory for electrolytes of unsymmetrical valence types, *J. Chem. Phys.*, *21*(6), 1054-1060.

Gregory, J. (1975), Interaction of unequal double layers at constant charge, *J. Colloid Interface Sci.*, *51*(1), 44-51.

Haines, W. B. (1930), Studies in the physical properties of soil, V. The hysteresis effect in capillary properties, and the modes of moisture distribution associated therewith, *Journal of Agricultural Science*, *20*, 97-116.
Hiemenz, P. C., and R. Rajagopalan (1997), *Principles of Colloid and Surface Chemistry, Third Edition, Revised and Expanded*, 3rd ed., 650 pp., Marcel Dekker, Inc., New York.
Hough, D. B., and L. R. White (1980), The calculation of Hamaker constants from Lifshitz theory with applications to wetting phenomena, *Adv. Colloid Interface Sci.*, *14*, 3-41.
Hu, Q. H., and J. S. Y. Wang (2003), Aqueous-phase diffusion in unsaturated geologic media: A review, *Crit. Rev. Env. Sci. Technol.*, *33*(3), 275-297.
Israelachvili, J. N., and D. Tabor (1972), The measurement of van der Waals dispersion forces in the range of 1.5 to 130 nm, *Proceedings of the Royal Society of London Series A.*, *331*, 19-38.
Israelachvili, J. N. (1991), *Intermolecular and Surfaces Forces*, 2nd ed., 450 pp., Academic Press, London.
Iwamatsu, M., and K. Horii (1996), Capillary condensation and adhesion of two wetter surfaces, *J. Colloid Interface Sci.*, *182*, 400-406.
Kitamura, A., K. Fujiwara, T. Yamamoto, S. Nishikawa, and H. Moriyama (1999), Analysis of adsorption behavior of cations onto quartz surface by electrical double-layer model, *J. Nucl. Sci. Technol.*, *36*(12), 1167-1175.
Langmuir, I. (1938a), Repulsive forces between charged surfaces in water, and the cause of the Jones-Ray effect, *Science*, *88*, 430-432.
Langmuir, I. (1938b), The role of attractive and repulsive forces in the formation of tactoids, thixotropic gels, protein crystals and coacervates, *J. Chem. Phys.*, *6*, 873-896.
Lebeau, M., and J.-M. Konrad (2010), A new capillary and thin film flow model for predicting the hydraulic conductivity of unsaturated porous media, *Water Resour. Res.*, *46*, W12554.
Li, H., X. Peng, L. Wu, M. Jia, and H. Zhu (2009), Surface potential dependence of the Hamaker constant, *Journal of Physical Chemistry C*, *113*(11), 4419-4425.
Low, P. F. (1987), Structural component of the swelling pressure of clays, *Langmuir*, *3*(1), 18-25.
Lyklema, J., and J. F. L. Duval (2005), Hetero-interaction between Gouy-Stern double layers: Charge and potential regulation, *Adv. Colloid Interface Sci.*, *114-115*, 27-45.
Maurice, P. A., M. F. Hochella, G. A. Parks, G. Sposito, and U. Schwertmann (1995), Evolution of Hematite Surface Microtopography Upon Dissolution by Simple Organic-Acids, *Clays Clay Miner.*, *43*(1), 29-38.
Melrose, J. C. (1966), Model calculations for capillary condensation, *A. I. Ch. E. Journal*, *12*(5), 986-994.
Miller, E. E., and R. D. Miller (1956), Physical theory for capillary flow phenomena, *J. Appl. Phys.*, *4*, 324-332.
Miyamoto, T., T. Annaka, and J. Chikushi (2005), Extended dual composite sphere model for determining dielectric permittivity of andisols, *Soil Science Society America Journal*, *69*(1), 23-29.
Najafi, A. S., J. Drelich, A. Yeung, Z. Xu, and J. Masliyah (2007), A novel method of measuring electrophoretic mobility of gas bubbles, *J. Colloid Interface Sci.*, *308*, 344-350.
Nimmo, J. R. (2010), Theory for source-responsive and free-surface film modeling of unsaturated flow, *Vadose Zone Journal*, *9*, 295-306.

Ninham, B. W. (1999), On progress in forces since the DLVO theory, *Adv. Colloid Interface Sci.*, *83*(1-3), 1-17.
Novich, B. E., and T. A. Ring (1985), Photon correlation spectroscopy of a coagulating suspension of illite platelets, *Journal of the Chemical Society, Faraday Transactions 1*, *81*, 1455-1457.
Novy, R. A., P. G. Toledo, H. T. Davis, and L. E. Scriven (1989), Capillary dispersion in porous media at low wetting phase saturations, *Chem. Eng. Sci.*, *44*(9), 1785-1797.
Ohshima, H., T. W. Healy, and L. R. White (1982), Improvement on the Hogg-Healy-Fuerstenau Formulas for the Interaction of Dissimilar Double-Layers. 1. 2nd and 3rd Approximations for Moderate Potentials, *J. Colloid Interface Sci.*, *89*(2), 484-493.
Or, D., and M. Tuller (1999), Liquid retention and interfacial area in variably saturated porous media: Upscaling from single-pore to sample-scale model, *Water Resour. Res.*, *35*(12), 3591-3605.
Or, D., and M. Tuller (2000), Flow in unsaturated fractured porous media: Hydraulic conductivity of rough surfaces, *Water Resour. Res.*, *36*, 1165-1177.
Orchiston, H. D. (1953), Adsorption of water vapor: I. Soils at 25˚C, *Soil Science*, *76*, 453-465.
Overbeek, J. T. G. (1990), The role of energy and entropy in the electrical double layer, *Colloids and Surfaces*, *51*, 61-75.
Philip, J. R. (1978), Adsorption and capillary condensation on rough surfaces, *J. Phys. Chem.*, *82*, 1379-1385.
Ponizovsky, A. A., S. M. Chudinova, and Y. A. Pachepsky (1999), Performance of TDR calibration models as affected by soil texture, *Journal of Hydrology*, *218*, 35-43.
Quirk, J. P. (1955), Significance of surface areas calculated from water vapor sorption isotherms by use of the B.E.T. equation, *Soil Science*, *80*(6), 423-430.
Read, A. D., and J. A. Kitchener (1969), Wetting films on silica, *J. Colloid Interface Sci.*, *30*(3), 391-398.
Russel, W. B., D. A. Saville, and W. R. Schowalter (1989), *Colloidal Dispersions*, 525 pp., Cambridge University Press, Cambridge.
Saiers, J. E., and J. J. Lenhart (2003), Colloid mobilization and transport within unsaturated porous media under transient-flow conditions, *Water Resour. Res.*, *39*(1), 1019.
Shang, J. Y., M. Flury, G. Chen, and J. Zhuang (2008), Impact of flow rate, water content, and capillary forces on in situ colloid mobilization during infiltration in unsaturated sediments, *Water Resour. Res.*, *44*, W06411.
Sposito, G. (1981), *The Thermodynamics of Soil Solutions*, 223 pp., Clarendon, Oxford.
Sposito, G. (1998), On points of zero charge, *Environ. Sci. Technol.*, *32*(19), 2815-2819.
Sweeney, J. B., T. Davis, and L. E. Scriven (1993), Equilibrium thin films on rough surfaces. 1. Capillary and disjoining effects, *Langmuir*, *9*(6), 1551-1555.
Takahashi, M. (2005), zeta potential of microbubbles in aqueous solutions: Electrical properties of the gas-water interface, *J. Phys. Chem. B*, *109*(46), 21858-21864.
Teng, H. H. (2004), Controls by saturation state on etch pit formation during calcite dissolution, *Geochim. Cosmochim. Acta*, *68*(2), 253-262.
Tokunaga, T. K., and J. Wan (1997), Water film flow along fracture surfaces of porous rock, *Water Resour. Res.*, *33*, 1287-1295.
Tokunaga, T. K., and J. Wan (2001), Approximate boundaries between different flow regimes in fractures rocks., *Water Resour. Res.*, *37*, 2103-2111.

Tokunaga, T. K., K. R. Olson, and J. Wan (2004), Conditions necessary for capillary hysteresis in porous media: Tests of grain size and surface tension influences, *Water Resour. Res.*, *40*, WO5111.
Tokunaga, T. K. (2009), Hydraulic properties of adsorbed water films in unsaturated porous media, *Water Resour. Res.*, *45*, W06415.
Tuller, M., D. Or, and L. M. Dudley (1999), Adsorption and capillary condensation in porous media: Liquid retention and interfacial configurations in angular pores, *Water Resour. Res.*, *35*(7), 1949-1964.
Tuller, M., and D. Or (2005), Water films and scaling of soil characteristic curves at low water contents, *Water Resour. Res.*, *41*, W09403.
Verwey, E. J. W., and J. T. G. Overbeek (1948), *Theory of the Stability of Lyophobic Colloids*, 218 pp., Dover Publications, Mineola, NY.
Viani, B. E., P. F. Low, and C. B. Roth (1983), Direct measurement of the relation between interlayer force and interlayer distance in the swelling of montmorillonite, *J. Colloid Interface Sci.*, *96*(1), 229-244.
Wan, J., and T. K. Tokunaga (1997), Film straining of colloids in unsaturated porous media: Conceptual model and experimental testing, *Environ. Sci. Technol.*, *31*, 2413-2420.
Wan, J., and T. K. Tokunaga (2002), Partitioning of clay colloids at air-water interfaces, *J. Colloid Interface Sci.*, *247*, 54-61.
Welzen, J. T. A. M., H. N. Stein, J. M. Stevels, and C. A. M. Siskens (1981), The influence of surface-active agents on kaolinite, *J. Colloid Interface Sci.*, *81*(2), 455-467.

Tables (total of 1)

Table 1. Hamaker constants (A_{11}) of oxides, aluminosilicates, and other common soil minerals reported in the literature, and their calculated nonretarded A_{132} for water films. *Values of A_{11} derived from aqueous suspension A_{131} measurements were estimated using the combining relation, $A_{11} \approx \left(\sqrt{A_{131}} + \sqrt{A_{33}}\right)^2$, with A_{33}(water) = 3.7×10^{-20} J.

solid phase	source	A_{11}, J	A_{132}, J
SiO_2	[*Derjaguin et al.*, 1978]	5×10^{-20}	-6×10^{-21}
SiO_2	[*Hough and White*, 1980]	6.55×10^{-20}	-1.0×10^{-20}
SiO_2	[*French*, 2000]	6.8×10^{-20}	-1.3×10^{-20}
Al_2O_3	[*French*, 2000]	1.65×10^{-19}	-4.1×10^{-20}
α-Al_2O_3	[*Hough and White*, 1980]	1.56×10^{-19}	-3.9×10^{-20}
α-Al_2O_3	[*Bergstrom*, 1997]	1.52×10^{-19}	-3.8×10^{-20}
α-FeOOH (goethite)	[*Blakey and James*, 2003]	$1.8 \times 10^{-19*}$	-4.5×10^{-20}
TiO_2	[*French*, 2000]	1.49×10^{-19}	-3.7×10^{-20}
muscovite mica	[*Israelachvili and Tabor*, 1972]	1.35×10^{-19}	-3.4×10^{-20}
muscovite mica	[*Hough and White*, 1980]	1.0×10^{-19}	-2.4×10^{-20}
illite	[*Novich and Ring*, 1985]	$1.8 \times 10^{-19*}$	-4.5×10^{-20}
kaolinite	[*Welzen et al.*, 1981]	$1.25 \times 10^{-19*}$	-3.1×10^{-20}
kaolinite	[*Berka and Rice*, 2004]	$1.67 \times 10^{-19*}$	-4.2×10^{-20}
montmorillonite, lowest potential	[*Li et al.*, 2009]	$1.09 \times 10^{-19*}$	-2.6×10^{-20}
montmorillonite, highest potential	[*Li et al.*, 2009]	$1.98 \times 10^{-19*}$	-4.9×10^{-20}
$CaCO_3$	[*Hough and White*, 1980]	$1.2 \times 10^{-19*}$	-2.9×10^{-20}
$CaCO_3$	[*Bergstrom*, 1997]	$1.2 \times 10^{-19*}$	-2.4×10^{-20}
soils (fit to moisture characteristics)	[*Or and Tuller*, 1999]	-	-6×10^{-20}

Figures (total of 9 figures)

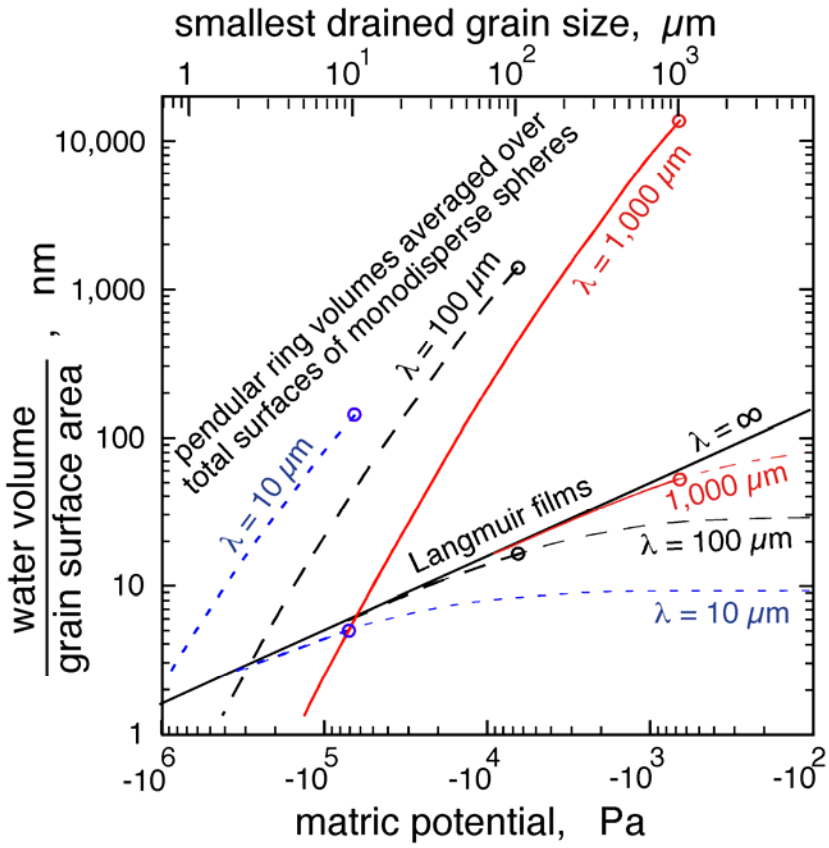

Figure 1. Comparisons of grain surface area normalized water volumes on close-packs of monodisperse spherical grains of different diameters (λ), based on pendular ring volumes and Langmuir's adsorbed film model for substrates with high electrostatic surface potential. Upper limits of all curves terminate at the condition where pendular rings become interconnected, and are indicated by circles. Extensions of the Langmuir curves to higher (less negative) energies depict film thicknesses on isolated grains, but are not applicable in porous media because pores become saturated. The upper x-axis on this and later graphs indicates the smallest spherical grain size in close packing in which pores are drained and pendular rings are discontinuous. The water-air surface tension is taken as 73 mN m^{-1} and contact angle is zero.

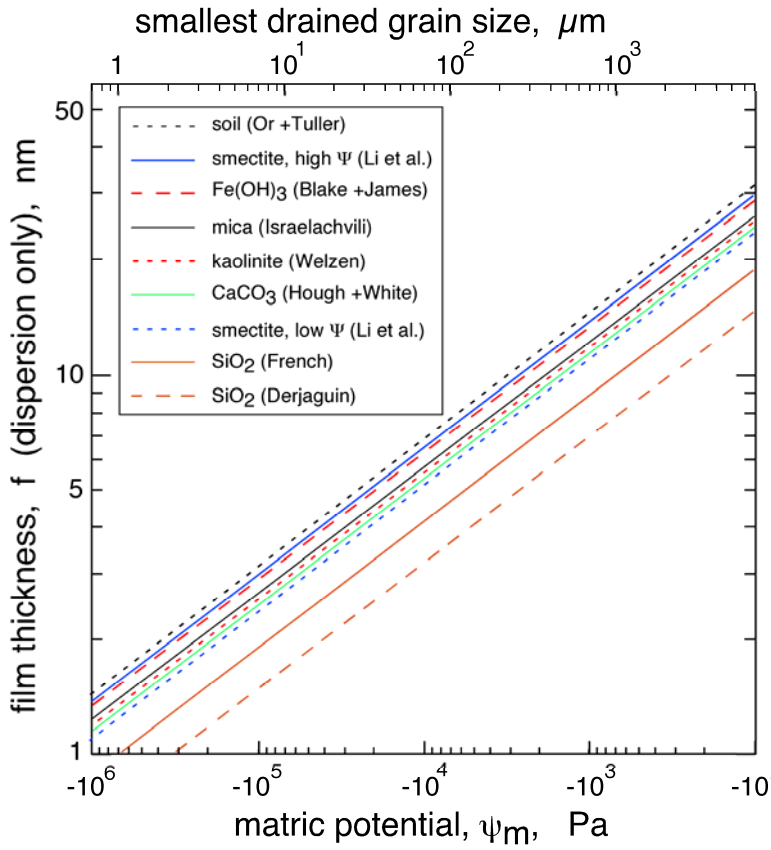

Figure 2. Predicted matric potential dependence of water film thicknesses on various common mineral surfaces, based solely on van der Waals interactions (equation (3a)) and Hamaker constants (A_{132}) listed in Table 1. The upper x-axis indicates the approximate smallest grain size allowing adsorption-dominated films. Pores in smaller grain size systems are capillary-filled.

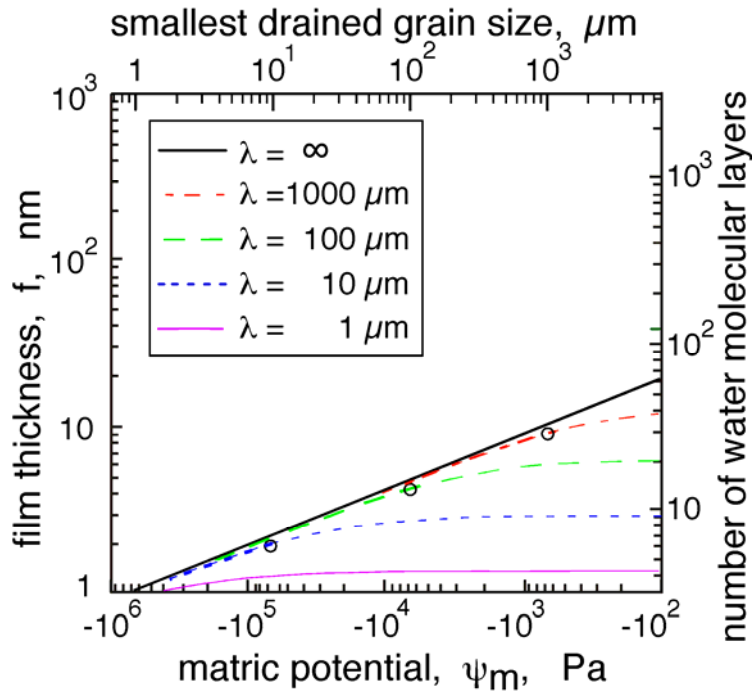

Figure 3. Predicted matric potential dependence and grain size dependence of water film thicknesses on SiO_2 surfaces, based solely on van der Waals interactions ($A_{132} = -1.3 \times 10^{-20}$) and surface tension (equation (3b)). The planar surface limit is given by the $\lambda = \infty$ curve (equation (3a)). Other curves are for spherical grains, with circles indicating the condition for pendular ring merging (wetting curves).

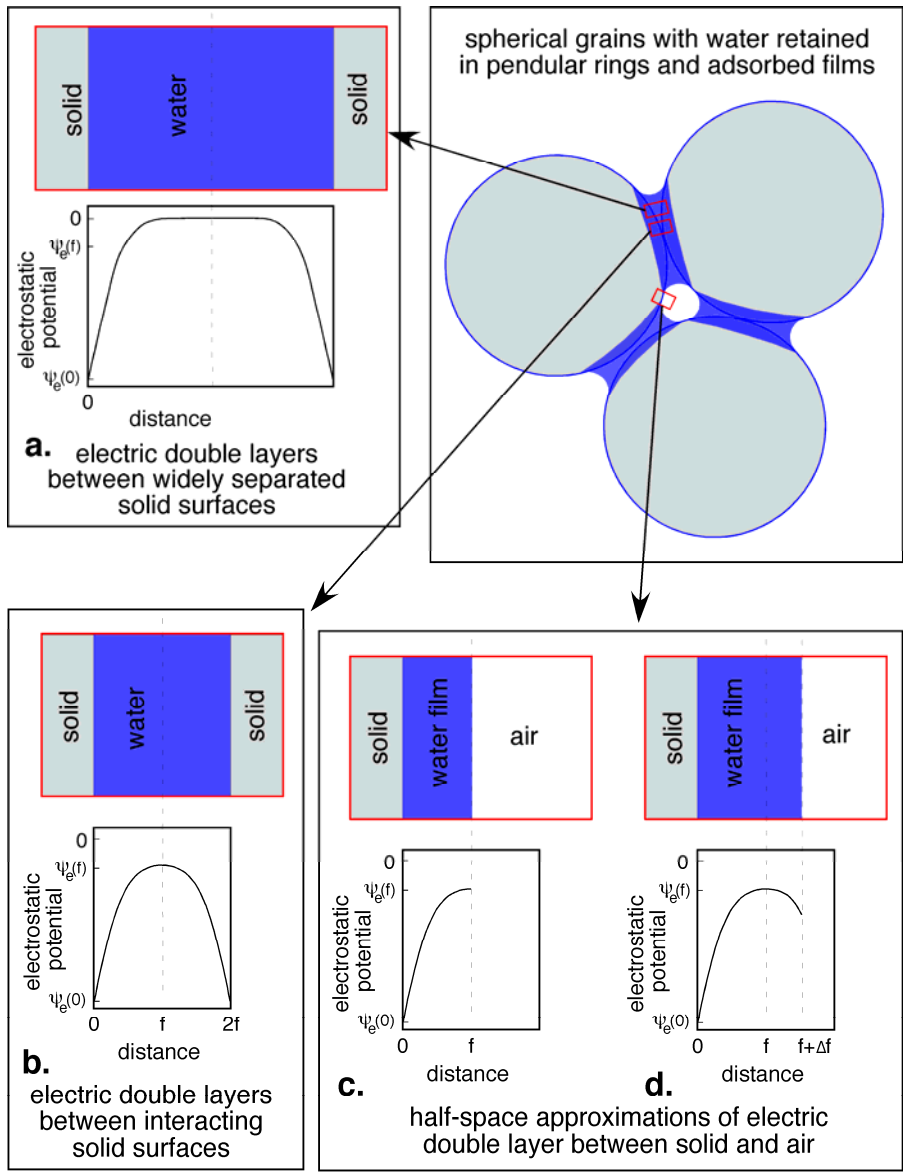

Figure 4. Configurations of water in unsaturated porous media, and associated electrostatic potential profiles. (a.) regions of thick capillary films between widely separated solid surface. (b.) regions of thinner water films confined between opposing solid surfaces with overlapping electric double layers. (c.) regions with adsorbed water films with negligible electrostatic potential gradient at the air-water interface. (d.) regions with adsorbed water films with finite electrostatic potential gradient at the air-water interface.

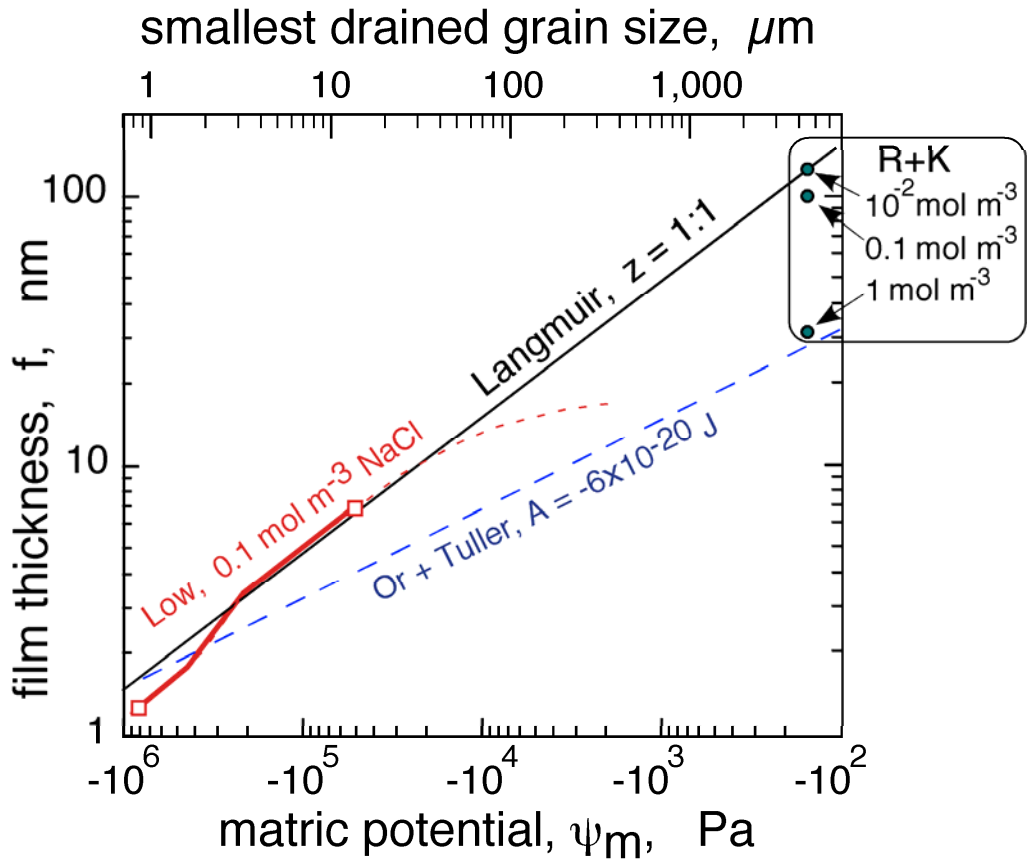

Figure 5. Comparison of Langmuir-model (equation (6)) for dilute 1:1 aqueous film thicknesses (solid black curve), Low's [*Low*, 1987] empirical relation (equation (7)) for smectite interlayer half-space thickness saturated with 10^{-1} mol m^{-3} KCl (red curve), and predictions based an effective Hamaker constant of -6×10^{-20} J (equation (3a)) [*Or and Tuller*, 1999]. The open squares on Low's regression equation represent lower and upper limits of the experimental results [*Viani et al.*, 1983]. "R+K" denote data for KCl solutions adsorbed on silica [*Read and Kitchener*, 1969].

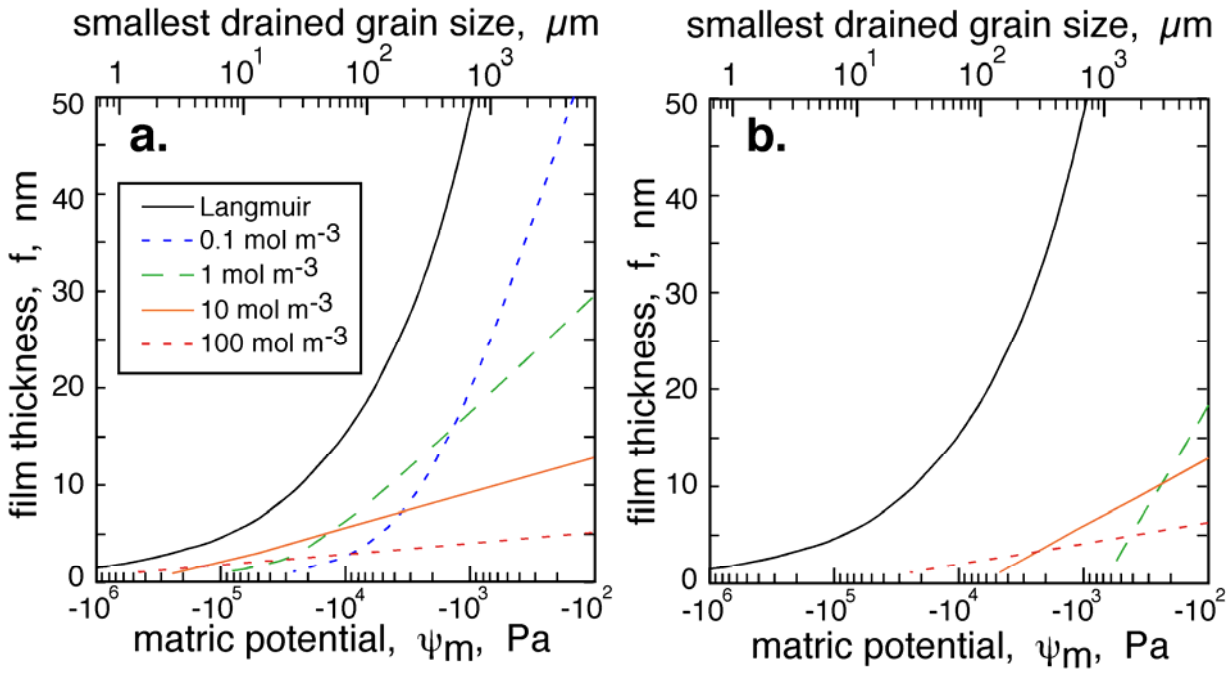

Figure 6. Matric potential dependence of water film thicknesses at different concentrations of a 1:1 electrolyte on a solid surface with ψ_e = -50 mV, from electrostatic interactions predicted by (**a.**) the compression model (equation (8)), and (**b.**) the LSA (equation (9)). Note that ψ_e for the air-water interface is set to 0 mV in the Langmuir and compression models, and -1 mV for the LSA cases shown here.

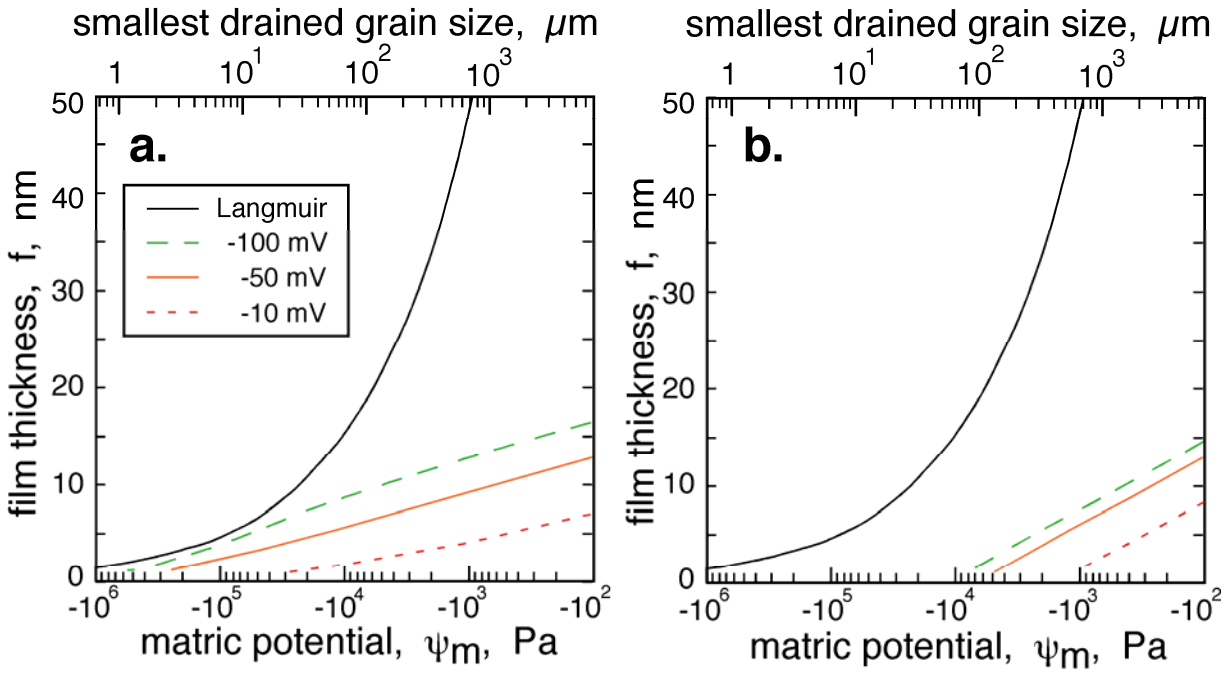

Figure 7. Matric potential dependence of water film thicknesses at different ψ_e at a solid surface, with 10 mol m^{-3} ionic strength, predicted by electrostatic interactions of (**a.**) the compression model (equation (8)), and (**b.**) the LSA (equation (9)). Note that ψ_e for the air-water interface is set to 0 mV in the Langmuir and compression models, and -1 mV for the LSA cases shown here.

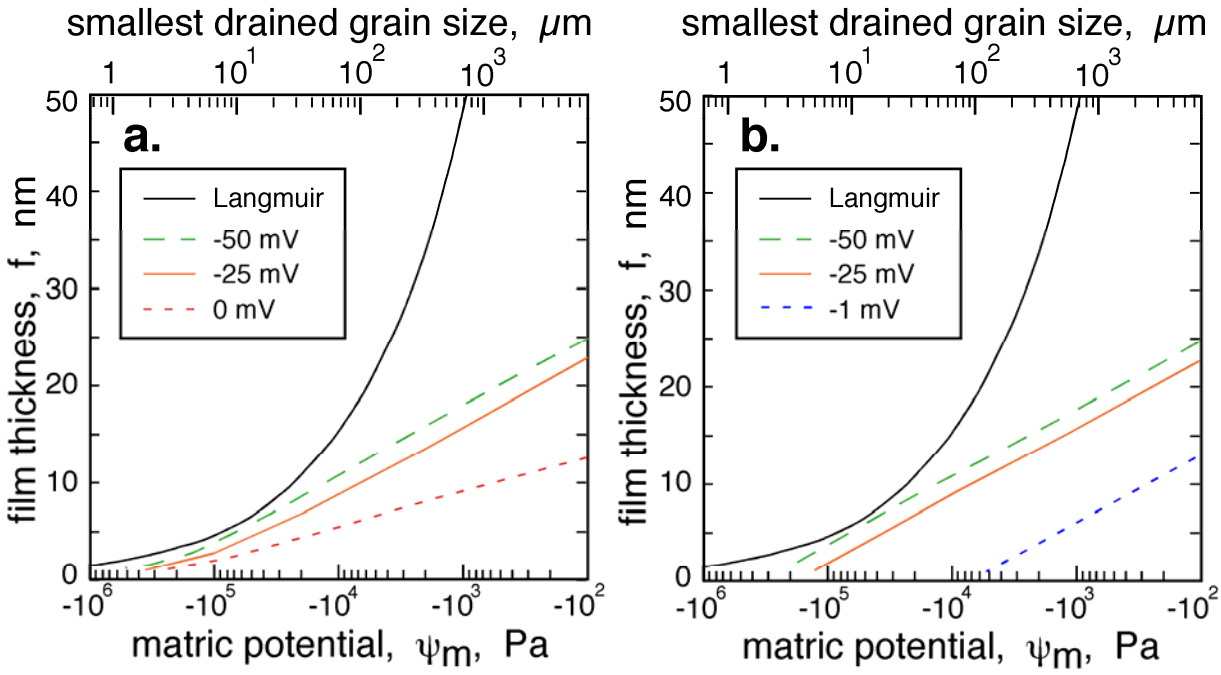

Figure 8. Matric potential dependence of water film thicknesses at 10 mol m^{-3} ionic strength, for a solid surface with ψ_e = -50 mV, and different values of ψ_e for the air-water interface, predicted by electrostatic interactions estimated from (**a.**) the compression model (equation (8)), and (**b.**) the LSA (equation (9)).

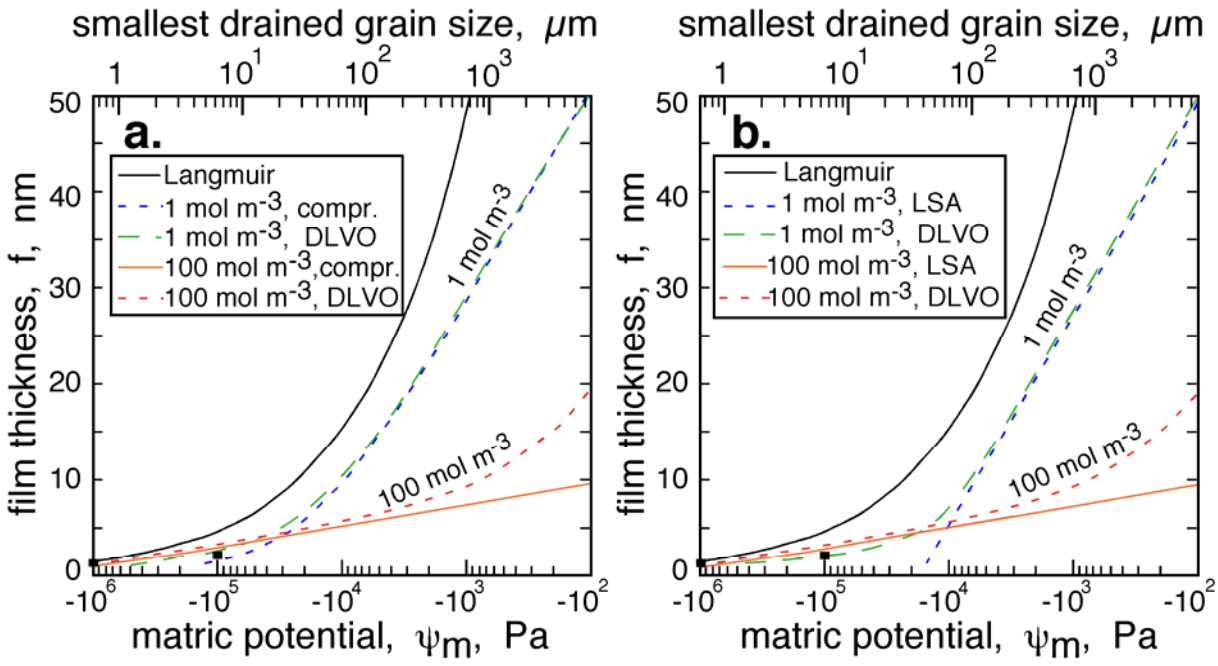

Figure 9. Matric potential dependence of water film thicknesses with $\psi_{e,1}$ = -50 mV, $\psi_{e,2}$ = -25 mV, and A_{132} = -1.3 x10^{-20} J, for 1 mol m^{-3} and 100 mol m^{-3} background ionic strength solutions, based on (**a.**) the compression model (equation (8)), and (**b.**) the LSA (equation (9)). The DLVO curves in these figures result from adding the van der Waals pressure component to the corresponding electrostatic pressure component following equation (11). The data points at -10^5 and -10^6 Pa are calculated film thicknesses based on soil moisture characteristics by Campbell and Shiozawa, and specific surface areas by Tuller and Or for the same 5 soils.